Human Cell (2024) 37:1378–1393
https://doi.org/10.1007/s13577-024-01086-7

RESEARCH ARTICLE

Delivery of neurotrophin-3 by RVG-Lamp2b-modified mesenchymal stem cell-derived exosomes alleviates facial nerve injury

Wenting Bi[1] · Xiaodan Mu[2] · Yongfeng Li[3] · Qingyan Sun[4] · Lei Xiang[5] · Min Hu[4] · Huawei Liu[4]

Received: 6 January 2024 / Accepted: 24 April 2024 / Published online: 11 June 2024
© The Author(s) under exclusive licence to Japan Human Cell Society 2024

Abstract

We aim to investigate the effect of RVG-Lamp2b-modified exosomes (exos) loaded with neurotrophin-3 (NT-3) on facial nerve injury. Exos were collected from control cells (Ctrl Exo) or bone marrow mesenchymal stem cells co-transfected with RVG-Lamp2b and NT-3 plasmids (RVG-NT-3 Exo) by gradient centrifugation and identified by western blotting, transmission electron microscopy, and nanoparticle tracking analysis. Effect of RVG-NT-3 Exo on oxidative stress damage was determined by analysis of the morphology, viability, and ROS production of neurons. Effect of RVG-NT-3 Exo on facial nerve axotomy (FNA) was determined by detecting ROS production, neuroinflammatory reaction, microglia activation, facial motor neuron (FMN) death, and myelin sheath repair. Loading NT-3 and modifying with RVG-Lamp2b did not alter the properties of the exos. Moreover, RVG-NT-3 Exo could effectively target neurons to deliver NT-3. Treatment with RVG-NT-3 Exo lowered H_2O_2-induced oxidative stress damage in primary neurons and Nsc-34 cells. RVG-NT-3 Exo treatment significantly decreased ROS production, neuroinflammatory response, FMN death, and elevated microglia activation and myelin sheath repair in FNA rat models. Our findings suggested that RVG-NT-3 Exo-mediated delivery of NT-3 is effective for the treatment of facial nerve injury.

Keywords Facial paralysis · NT-3 · RVG-Lamp2b · Facial motor neuron · Microglia

Introduction

Facial paralysis is mainly caused by facial nerve damage leading to facial muscle paralysis, and its typical symptoms include crooked corners of the mouth and air leakage during speech [1]. This disease causes significant damage to the physical and mental health of patients, resulting in a decrease in their quality of life [2, 3]. Drugs such as dexamethasone, mannitol, and B vitamins are commonly used clinically to treat facial nerve palsy, which reduces symptoms of inflammation and local edema of damaged nerves but is less effective in facial recovery [4]. Therefore, it is

Wenting Bi and Xiaodan Mu are co-first authors.

✉ Huawei Liu
liuhuawei840222@126.com

Wenting Bi
biwenting2008@126.com

Xiaodan Mu
18510619655@163.com

Yongfeng Li
liyongfeng28@sina.com

Qingyan Sun
1031283321@qq.com

Lei Xiang
xianglei-322@163.com

Min Hu
humin48@vip.163.com

[1] Department of Stomatology, Beijing Hospital of Integrated Traditional Chinese and Western Medicine, Beijing 100000, China

[2] Department of Stomatology, Beijing Friendship Hospital, Capital Medical University, Beijing 100000, China

[3] Department of Stomatology, School of Clinical Medicine, Beijing Tsinghua Changgung Hospital, Tsinghua University, Beijing 102200, China

[4] Department of Stomatology, The First Medical Center, Chinese PLA General Hospital, No.28 Fuxing Road, Haidian District, Beijing 100853, China

[5] Beijing Research Institute of Traumatology and Orthopaedics, Beijing 102200, China

necessary to actively explore new treatment strategies for better treatment of facial nerve palsy.

The successful regeneration of peripheral nerves mainly depends on the regulation of neuronal survival and axon regeneration by the regenerative microenvironment, and neurotrophins mainly play a decisive role in the regenerative microenvironment [5]. To exert their effects, neurotrophins are transported to neuronal somas via retrograde axons through binding to the corresponding specific receptors [6, 7]. Neurotrophin-3 (NT-3), a member of the neurotrophin family, is extremely important for the development, maturation, and regeneration of the nervous system [8]. Studies have shown that NT-3 is essential for the development and maturation of the nervous system, including the regulation of neuronal survival, axon growth, synaptic plasticity, and neurotransmission [9–11]. Also, the combination of surgical reconstruction and NT-3 gene therapy has been reported to be promising for the treatment of facial paralysis in humans [12]. NT-3 fused with a collagen-binding domain enhances facial nerve regeneration and functional recovery [13]. These data shed light on the importance of exogenous NT-3 delivery in repairing facial nerve damage. Some delivery systems of NT-3 have been established for other diseases, such as adeno-associated virus-mediated NT-3 for Charcot–Marie–Tooth disease and NT-3/fibroin coated gelatin sponge scaffold for spinal cord injury [14, 15]. However, adeno-associated virus vectors have a drawback of the delay of transgene expression for gene delivery applications [16]; while the administration way of gelatin sponge scaffold is not suitable for general facial paralysis treatment. Therefore, it is of great significance to efficiently develop a new NT-3 delivery system for facial paralysis.

Exosomes (Exos), nanoscale membranous vesicles with a particle size of 40–100 nm, are released from cells and can be precipitated by high-speed centrifugation (100,000 × g) [17]. Exos have high biocompatibility and low immunogenicity, which makes them have great potential for transporting nucleic acid sequences and drugs [18, 19]. Recently, exos derived from mesenchymal stem cells (MSCs) exhibited a superior benefit for facial nerve injury recovery, supporting the therapeutic potential of exos in facial paralysis [20]. The natural exos modified through biotechnology can enhance their drug delivery, targeting, and slowing down aggregation and protein adsorption capabilities [21]. For example, a previous study revealed that exos isolated from human umbilical cord MSCs are more effective in myocardial infarction therapy after increasing the content of platelet-derived growth factor D by Akt modification with human umbilical cord MSCs [22]. Besides, Tamura et al. applied the cationized pullulan to modify the surface of exos, thereby enhancing their targeted ability and therapeutic effect to the injured liver [23].

To make the exos have neuron-specific targeting ability, researchers have engineered the rabies virus glycoprotein (RVG) that can specifically bind to the acetylcholine receptor (AchR) into the exos membrane by fusing it into the lysosome-associated membrane glycoprotein 2b (Lamp2b) [24]. Several studies reported that using exos derived from bone marrow MSCs modified with RVG-Lamp2b could promote the targeted delivery of gene drugs to the brain [25, 26]. Therefore, we supposed that modifying MSC-derived exos with RVG-Lamp2b could improve the delivery efficacy of NT-3, thereby promoting its therapeutic efficiency on facial paralysis. In the present study, we extracted exos from bone marrow MSCs co-transfected with RVG-lamp2b and NT-3 to explore the efficacy of RVG-lamp2b and NT-3-modified exos in the treatment of facial paralysis.

Materials and methods

Cell culture

Rat bone marrow MSCs purchased from Procell (Cat#CP-R131, Wuhan, China) were cultured in α-MEM medium (Cat#41,061,037, Gibco, USA) containing 10% fetal bovine serum (FBS) (Cat#G8001, Servicebio, Wuhan, China) and 1% penicillin/streptomycin (Cat# PB180120, penicillin/streptomycin, Procell). The motor neuron-like cell line Nsc-34, a hybrid cell line generated by the fusion of mouse spinal cord neurons and mouse neuroblastoma purchased from MINGZHOUBIO. (Cat#MZ-0662, Ningbo, China), was cultured in EMEM (Cat#ZQ-301, Zhong Qiao Xin Zhou Bio., Shanghai, China), which was widely used in studying pathophysiology of motor neurons [27]. All cells were maintained at 37˚C in the humidified incubator with 95% relative humidity and 5% carbon dioxide. The experiments were performed on cells between passages 2 and 4.

Isolation and cultivation of primary neurons

Cerebral cortical neurons were obtained from the brains of neonatal Sprague–Dawley rats (Chengdu Dossy Experimental Animals Co., Ltd., Chengdu, China) within 24 h as previously described [28]. Briefly, the removed brain tissues were placed on 35 mm glass petri dishes containing ice-cold D-Hanks (2 mL, Cat#H9394, Sigma, St. Louis, MO, USA) and cut into tiny particles, followed by digestion with trypsin (Cat#25,200,072, Livning, Beijing, China) for 20 min at 37˚C. The cortex was easily dissociated by triturating in DMEM/F12 (Cat#C11330500BT, Gibco) containing 10% FBS. After pipetting, the cells (1×10^6 /mL) were planted in 96-well plates coated with 100 mg/L poly-L-lysine and incubated at 37˚C in a humidified incubator containing 5% carbon dioxide for 4 h. Then, the cells were incubated in

serum-free neurobasal A medium (Cat#10,888,022, Gibco) supplemented with 2% B27 (Cat#12,587–010, Gibco), 5 μmol/L glutamine (Cat#G0200, Solarbio, Beijing, China), 100 U/mL penicillin (Cat#PB180120, Procell), and 100 U/mL streptomycin (Cat#PB180120, Procell). Cytosine arabinoside (2.5 mg/L, Cat#C1768, Sigma) was supplemented and incubated for 24 h to suppress the growth of glial cells on day 3. Cell purity was checked by staining the cells with toluidine blue.

Transfection and preparation of exos

The pcDNA GNSTM-3-RVG-10-Lamp2b-HA (RVG-Lamp2b) (Cat#71,294, Addgene, Watertown, MA, USA) and pLV-NT-3/D15A (NT-3) (Cat#73,035, Addgene) plasmids were diluted in Opti-MEM (Cat#51,985,091, Gibco) and co-transfected into bone marrow MSCs using Lipofectamine 2000 (Cat#11,668,500, Invitrogen, Carlsbad, CA, USA) according to the manufacturer's recommended protocols.

For the isolation of exos, the transfected bone marrow MSCs were cultured under standard conditions. At 70–80% confluency, bone marrow MSCs were washed and then cultured in a completely fresh medium supplemented with 10% Exo-deficient FBS (Cat#Exo-FBS-250A-1, SBI System Biosciences, USA) for 48 h. Then, the conditioned medium was collected and used for exo isolation. As described in the report [29], exos were obtained by gradient centrifugation using an L-80XP supercentrifuge (Beckman Colter Optima L-100XP, Beckman Corter). First, the collected conditioned medium was subjected to sequential ultracentrifugation at 2000 g for 10 min at 4 °C to remove cell debris and then passed through 0.22 μm filters, spun at 10,000 g for 30 min, then 100,000 g for 4 h at 4 °C. Exo pellets were resuspended in PBS washed once with PBS and resuspended for further characterization or stored at − 80 °C.

Exo characterization and analysis

For the identification of purified exos, western blotting was performed using antibodies against Tumor Susceptibility 101 (TSG101) (Cat#A01233, Boster, Guangzhou, China), CD63 (Cat#orb736293, Biorbyt, Wuhan, China), or CD9 (Cat#144–01703, RayBiotech, Guangzhou, China) to detect the characteristic membrane proteins of exos. For the observation of the morphology of exos, purified exos re-suspended in PBS were fixed with 3% glutaraldehyde solution (Cat#G5882, Sigma) for half an hour and added to a copper grid, and dyed with 1% phosphotungstic acid for 5 min at room temperature, followed by examination with a transmission electron microscopy (TEM) (Zeiss Libra 120, Zeiss, Germany) at 120 kV. Automatic tracking of the number and size of purified exos was performed by nanoparticle tracking analysis (NTA) using the NanoSight LM10-HSB instrument (A&P Instrument Co, United Kingdom). A high-resolution particle-size distribution was detected and processed with the NTA 2.2 Analytical Software Suite.

Reverse transcription-quantitative polymerase chain reaction (RT-qPCR)

Total RNA was extracted from exos using the Exo RNA Isolation Kit (Cat#58,000, Norgen Biotek, Thorold, ON, Canada) according to the manufacturer's instructions and then quantified using a DS-11 Series Spectrophotometer/Fluorometer (DeNovix, Wilmington, DE, USA). One microgram of total RNA was reverse-transcribed to complementary (c) DNA with the iScript Reverse Transcription Supermix (Cat#1,708,840, Bio-Rad, Hercules, CA, USA). For qPCR amplification, 5 ng of cDNA was amplified with specific primers using TaqMan Fast Advanced Master Mix (Cat#4,444,963, Thermo, Waltham, MA, USA). Using GAPDH as a reference gene, we calculated NT-3 mRNA expression with the $2^{-\Delta\Delta Ct}$ method [30]. The primers used were listed in Table 1.

Western blotting

Total protein was extracted from exos with the BBproExtra® Exo-IsolationTM (Cat#BB-396, Bestbio, Shanghai, China) and from tissue samples with RIPA lysis buffer containing protease inhibitor cocktail (Cat#P8340, Sigma) and phosphatase inhibitor cocktail (Cat#P0044, Sigma). Protein concentration was determined using the BCA assay (Cat#23,225, Thermo). Proteins were separated by SDS-PAGE and transferred to a nitrocellulose membrane (Cat#10,600,007, GE Healthcare, Logan, UT, USA). The membranes were incubated overnight with primary antibodies (Table 2). After washing, secondary antibodies were incubated for 1 h. Protein bands were visualized using SuperSignal TM West Dura Extended Duration Substrate (Cat#34,075, Thermo) or Femto Maximum Sensitivity Substrate (Cat#34,094, Thermo) and quantified by using Image J software (NIH, Bethesda, USA).

Table 1 Primer sequences

Gene	Sequence	
NT-3	Forward	CTCCTAAGGCAGCAGAGACG
	Reverse	AGCGGATGATTTGTCCGTGA
GAPDH	Forward	GAGAGTGTTTCCTCGTCCCG
	Reverse	ACTGTGCCGTTGAATTTGCC

Table 2 The antibodies used in this research

Antibody	Manufacturer	Cat.no
NT-3	MyBioSource.com	MBS841227
Lamp2b	MyBioSource.com	MBS9410702
CD81	GeneTex	GTX101766
TSG101	GeneTex	GTX70255
Iba1	GeneTex	GTX635399
iNOS	Proteintech Group Inc	18,985-1-AP
Arg1	Merck	SAB4200508
Myelin PLP	GeneTex	GTX134433
β3-tubulin	MyBioSource.com	MBS355132
GAPDH	Abcam	ab8245

Cell viability experiment

The viability of primary neurons and Nsc-34 cells with or without H_2O_2 stimulation (0.5 mM) was evaluated using Cell Counting Kit-8 (CCK-8, Beyotime, Shanghai, China). Cells (5×10^3 cells/well) were seeded into 96-well plates and stimulated with H_2O_2 for 8 h, followed by treatment with RVG-NT-3 Exo or Ctrl Exo (100 μg) for 24 h. Next, 10 μL of CCK-8 solution (Cat#CA1210, Ribobio, Guangzhou, China) was added into each well and incubated for 2 h. The absorbance was measured at 450 nm using a microplate reader (BioTek, Winooski, VT, USA).

Reactive oxygen species (ROS) experiment

The levels of intracellular ROS were determined using the ROS assay kit (Cat#S0033S, Beyotime) following the manufacturer's protocol. The peroxide-sensitive fluorescent probe 2,7-dichlorodihydrofluorescein diacetate (DCFH-DA) was used to measure the intracellular levels of ROS in primary neurons and Nsc-34 cells. Images of cells were captured with a confocal microscopy (FV3000, Olympus). The fluorescence intensity was quantified via Image-Pro Plus software (NIH).

Facial nerve axotomy (FNA)

Six-week-old male Sprague–Dawley rats (200–250 g) (Beijing Vital River Laboratory Animal Technology Co., Ltd.) were subjected to a 1-week quarantine and adaptation period. Rats were fed standard laboratory chow and water ad libitum and housed under an artificial 12-h light on/off cycle before and after surgery. This study was performed after being approved by the First Medical Center, Chinese PLA General Hospital Animal Care and Use Committee. According to previously published protocols, rat models of unilateral FNA at stylomastoid foramen were established. Briefly, rats were anesthetized by 10% chloral hydrate (3 mg/Kg, Cat#C8383, Sigma). A vertical incision (1 cm) was made along the retroauricular groove to expose the facial nerve trunk after the iodophor disinfection and skin preparation. The stylomastoid foramen was located along the nerve trunk. At the stylomastoid foramen, an ophthalmic tweezer was used to gently separate the facial nerve and pulled outside for 2 mm. Then, the facial nerve was cut off with ophthalmic shears, resulting in the FNA at a high position, followed by suturing the skin incision. For the sham operation, the skin incision was made and the facial nerve was exposed up to the stylomastoid foramen. No cut was made on the facial nerve. After surgery, the rat models were re-warmed in the incubator and then returned to the cage with regular feeding. The facial paralysis was observed every 24 h. After the surgery, due to the lack of blinking and rapid reflexes, it was confirmed that the facial nerve was cut off. For treatment, rats were administered with RVG-NT-3 Exo or Ctrl Exo (100 μg) via a single intravenous injection into the tail vein at days 0 and 7. Recovery of facial movements was tested weekly for 2 weeks after surgery. By blowing air onto the cornea, the eye closure ability was activated after the blink reflex. Movements were recorded with a video camera. Rats ($n = 5$) were euthanized at 14 days post-operation using CO_2 inhalation and cervical dislocation. Facial nerve samples were removed for subsequent analysis.

Enzyme-linked immunosorbent assay (ELISA)

The nerve samples were homogenized in cold PBS and the supernatants were collected. The levels of inflammatory cytokines IL-4 (Cat#PI615, Beyotime), IL-10 (Cat#PI525, Beyotime), IL-33 (Cat#ER1903, Finetest, Wuhan, China), TNF-α (Cat#PT516, Beyotime) and IL-6 (Cat#PI328, Beyotime) were assessed using rat ELISA kits according to the manufacturer's instructions.

Tunel staining

Tunel staining was performed using the One-step Tunel In Situ Apoptosis Kit (Green, FITC) (Cat#E-CK-A320 Elabscience, Wuhan, China) according to the manufacturer's instructions. In brief, paraffin-embedded rat nerve slices (4 μm thick) were deparaffinized in xylene (Cat#1330-20-7, Kbsys, China), rehydrated in gradient ethanol (Cat#64-17-5, Kbsys), incubated with Tunel reagent mixture for 60 min, counterstained with DAPI for 5 min and examined under a fluorescence microscope (Olympus). The Tunel index was calculated as the proportion (%) of Tunel-positive neurons among DAPI-positive neurons.

Nissl staining

Nissl staining was performed using the Nissl Stain Kit (methyl violet method) (Cat#G1432, Solarbio) following the manufacturer's instructions. Observation of the results was performed under an optical microscope (Olympus). Nissl-positive cells were calculated by analyzing 4 randomly selected high-power fields through Image-Pro Plus software (NIH).

Luxol fast blue (LFB) staining

The dewaxed slices were immersed for 3–4 h in the LFB staining buffer (A) (Cat#B0018, Powerful Biology, Wuhan, China) preheated for 30 min in a 60 °C oven. The slices were differentiated alternately in 70% ethanol (B) (Cat#B0018, Powerful Biology) and lithium carbonate solution (C) (Cat#B0018, Powerful Biology), and the differentiation was stopped by washing. The degree of differentiation was controlled under a microscope. Then slices were mounted with neutral gum (Cat#G8590, Solarbio). Photos were taken with an optical microscope (BX51, Olympus, Japan).

Statistical analysis

All data were presented as mean ± standard deviation (SD) and were analyzed by GraphPad Prism 8 (GraphPad Inc., La Jolla, CA, USA). The two-tailed Student's t-test was applied for comparison between two groups, one-way analysis of variance (ANOVA) with Bonferroni's post hoc test for multiple comparisons. $p < 0.05$ was considered statistically significant.

Results

Co-expression of RVG-lamp2b and NT-3 in bone marrow MSC-derived exos

To discuss the effect of bone marrow MSC-derived exos co-expressed with RVG-lamp2b and NT-3 on facial nerve injury, bone marrow MSCs were co-transfected with RVG-lamp2b and NT-3 plasmids to obtain stable cell strains. Exos derived from control bone marrow MSCs and bone marrow MSCs with RVG-Lamp2b + NT-3 were obtained by gradient centrifugation and named Ctrl Exo and RVG-NT-3 Exo respectively. Western blotting analysis of exo characteristic membrane proteins CD63, TSG101, and GM130 further confirmed the identity of the obtained particles Ctrl Exo and RVG-NT-3 Exo (Fig. 1B). As expected, the Lamp2b and NT-3 proteins were abundant in RVG-NT-3 Exo, while they were but not in Ctrl Exo (Fig. 1B). Through TEM, it could be seen that the electron density at the edges of Ctrl Exo and RVG-NT-3 Exo was higher than the inner densities, with a tea tray-like structure concave to one side, which is consistent with the basic morphology of exos (Fig. 1C). NTA detection of the particle size of Ctrl Exo and RVG-NT-3 Exo showed that their diameters were distributed between 50 and 150 nm, consistent with the diameter of exos (Fig. 1D). These results showed that there were no significant differences between the morphologies of Ctrl Exo and RVG-NT-3 Exo.

RVG-NT-3 Exo targeted neurons to deliver NT-3

To verify the ability of RVG-NT-3 Exo to target neurons, we incubated control bone marrow MSCs, primary neurons, and Nsc-34 cell lines with different concentrations of RVG-NT-3 Exo (0, 20, 50, and 100 μg). RT-qPCR results showed that the levels of NT-3 mRNA in primary neurons and Nsc-34 cells were increased with increasing concentration of incubated RVG-NT-3 Exo, while those in bone marrow MSCs had no obvious change (Fig. 2A). The levels of NT-3 protein in different cells treated with 100 μg of RVG-NT-3 Exo are shown in Fig. 2B. After co-incubation with RVG-NT-3 Exo, the levels of NT-3 protein in primary neurons and Nsc-34 cells were significantly higher than before incubation, but not in bone marrow MSCs. These results suggested that RVG-NT-3 Exo could target neurons to deliver NT-3.

RVG-NT-3 Exo effectively lowered H_2O_2-induced oxidative stress damage in neurons

To address the protective effect of RVG-NT-3 Exo on neuronal damage, primary neurons and Nsc-34 cells were stimulated with H_2O_2 (0.5 mM) and then treated with 100 μg of RVG-NT-3 Exo. Morphological observation was performed using a bright-field microscope. H_2O_2 stimulation caused the disappearance of synapses and cell contraction in primary neurons and Nsc-34 cells, which were weakened by RVG-NT-3 Exo or Ctrl Exo treatment, especially treatment with RVG-NT-3 Exo (Fig. 3A). Exposure of primary neurons and Nsc-34 cells to H_2O_2 for 8 h resulted in a decrease in cell viability to about half of the control, while treatment with RVG-NT-3 Exo and Ctrl-Exo significantly improved H_2O_2-induced reduction in cell viability (Fig. 3B and C). Stimulation of primary neurons and Nsc-34 cells to H_2O_2 elicited a threefold increase in ROS production compared to the control group, and ROS generation was attenuated significantly when cells were treated with RVG-NT-3 Exo or Ctrl-Exo (Fig. 3D and E). Collectively, these data manifested that RVG-NT-3 Exo could effectively ease H_2O_2-induced oxidative stress damage in neurons.

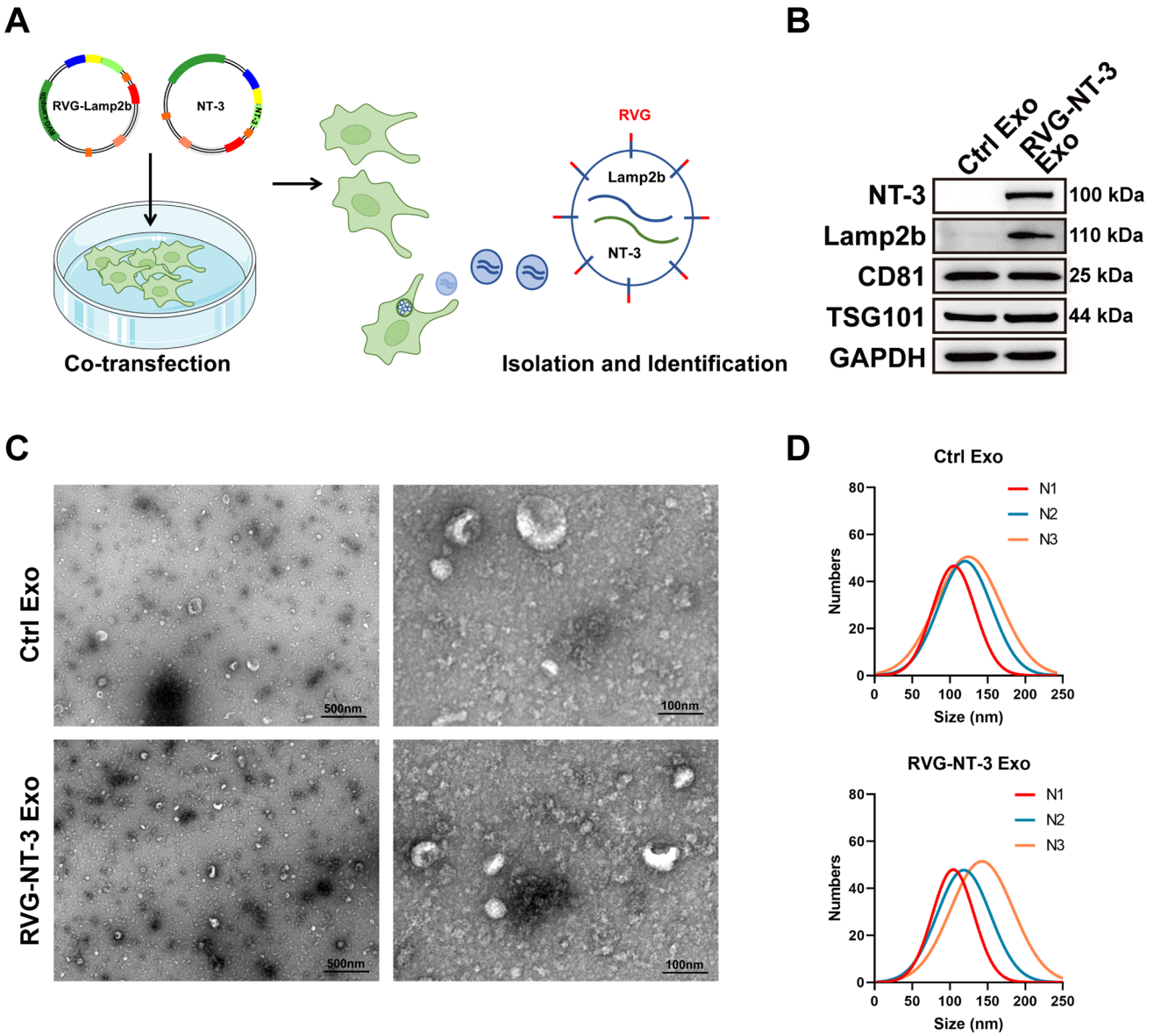

Fig. 1 Preparation and characterization of engineered RVG-NT-3 Exo. **A** Schematic diagram of the preparation of engineered RVG-NT-3 Exo. **B** Western blotting detection of the protein levels Lamp2b, NT-3, CD81, and TSG101 in Ctrl Exo and RVG-NT-3 Exo ($n=3$). **C** Representative TEM images of Ctrl Exo and RVG-NT-3 Exo ($n=3$). Scale bar, 100 nm or 500 nm. **D** NTA detection of the particle diameter of Ctrl Exo and RVG-NT-3 Exo ($n=3$)

RVG-NT-3 Exo reduced FNA-induced inflammation

To verify the protective effect of RVG-NT-3 Exo on neuronal damage, FNA rat models were constructed, followed by treatment with Ctrl Exo or RVG-NT-3 Exo. Supplementary Fig. 1A showed the flowchart of Ctrl-Exo or RVG-NT-3-Exo administration on the FNA rat model. Supplementary Figs. 1B and C displayed the structure of the facial nerve and related images of the FNA surgical process. The number of blinks per unit of time was used to evaluate the success of surgery, and the results showed that the number of blinks on the ipsilateral side of the injury was significantly smaller than on the contralateral side, indicating the successful construction of the FNA rat model (Supplementary Fig. 1D).

FNA rat models were administrated with Ctrl-Exo or RVG-NT-3-Exo at days 0 and 7. Rats were euthanized at 14 days to collect facial nerve samples to investigate the effects of Ctrl-Exo or RVG-NT-3-Exo on FNA-induced inflammation. The production of ROS was detected, and the results showed that FNA led to an increase in ROS production in facial nerve samples, while RVG-NT-3-Exo treatment significantly reduced ROS production instead of Ctrl

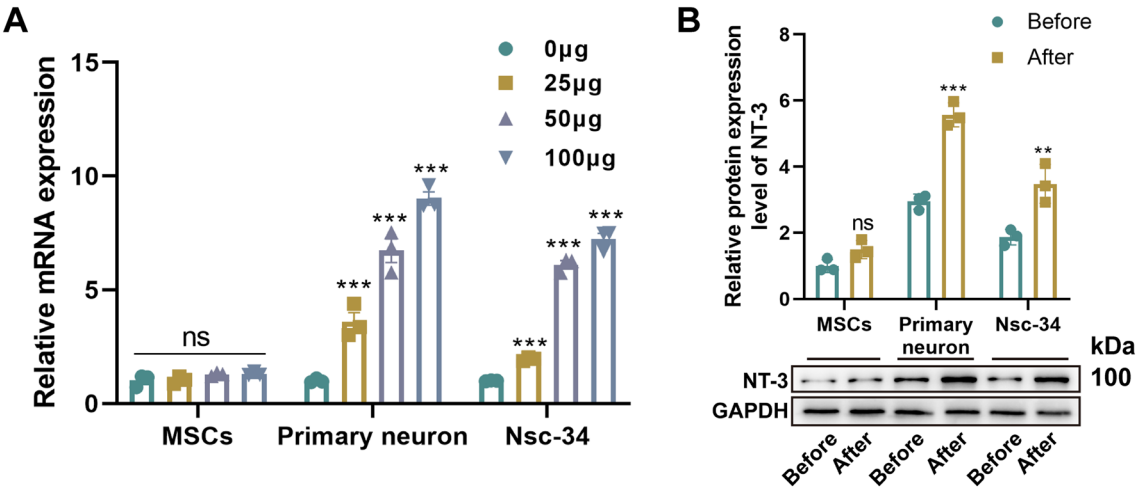

Fig. 2 RVG-NT-3 Exo effectively targeted neurons to deliver NT-3. **A** RT-qPCR detection of NT-3 mRNA levels in bone marrow MSCs, primary neurons, and Nsc-34 cell lines co-incubated with different concentrations of RVG-NT-3 Exo (0, 20, 50, and 100 μg) ($n=3$). **B** Western blotting analysis of NT-3 protein levels in bone marrow MSCs, primary neurons, and Nsc-34 cell lines co-incubated with 100 μg of RVG-NT-3 Exo ($n=3$). Statistical analysis was done by one-way ANOVA with multiple comparisons (**$p<0.01$ and ***$p<0.001$ vs. MSCs). All quantitative data are presented as mean ± SD

Exo treatment (Fig. 4A). ELISA showed that FNA significantly increased the release of pro-inflammatory cytokines TNF-α and IL-6 in facial nerve samples and reduced the release of anti-inflammatory cytokines IL-4, IL-10, and IL-33(Fig. 4B–F). The FNA-induced alterations in the release of inflammatory cytokines described above were significantly attenuated after RVG-NT-3-Exo treatment, while Ctrl Exo treatment only weakened the alterations in IL-10 (Fig. 4B–F). Microglial activation and polarization markers Iba1, iNOS (M1 type marker), and Arg1 (M2 type marker) were detected by western blotting (Fig. 4G). Figure 4G displayed that FNA increased Iba1 and iNOS protein levels, as well as decreased Arg1 protein levels, while RVG-NT-3-Exo treatment significantly attenuated the FNA-mediated effects on Iba1, iNOS, and Arg1 protein levels, but Ctrl Exo treatment did not, indicating that RVG-NT-3-Exo treatment promoted the polarization of microglia to the anti-inflammatory phenotype (M2). All outcomes manifested that RVG-NT-3 Exo could diminish FNA-induced inflammation.

RVG-NT-3 Exo reduced FNA-induced neuron apoptosis and facial motor neuron (FMN) death

Further experiments were carried out to discuss the effect of RVG-NT-3 Exo on reduced FNA-induced motor neuron apoptosis and death in facial nerve samples. Tunel staining showed that the number of Tunel-positive cells was higher in FNA-derived facial nerve samples, but RVG-NT-3 Exo treatment lowered the elevated number of Tunel-positive cells mediated by FNA rather than Ctrl-Exo treatment (Fig. 5A). Changes of Nissl bodies were determined by Nissl staining. As shown in Fig. 5B, FNA resulted in an overt decrease in the number of motor neurons, but RVG-NT-3 Exo treatment improved FNA-mediated reduction in the number of motor neurons. Together, RVG-NT-3 Exo reduced FNA-induced neuron apoptosis and FMN death.

RVG-NT-3 Exo promoted myelin sheath repair after facial nerve injury

Den-myelination of axons is an important factor causing neurological dysfunction after facial nerve injury, therefore promoting myelin sheath regeneration is crucial [31]. In the control group, the LFB staining was uniform and tightly arranged, while the LFB staining in the FNA group was messy and the number of myelinated nerve fibers was significantly reduced. After the treatment of Ctrl-Exo and RVG-NT-3-Exo, the myelin damage was weakened, which was manifested by an increase in the number of myelinated nerve fibers, and the treatment effect of RVG-NT-3-Exo was more pronounced than that of Ctrl-Exo (Fig. 6A). Myelin PLP and β3-tubulin proteins associated with myelin sheath were detected, and the results showed a significant reduction in Myelin PLP and β3-tubulin protein levels in facial nerve samples in the FNA group, while only RVG-NT-3-Exo treatment partially reversed the decreased levels of Myelin PLP and β3-tubulin protein (Fig. 6B). What's more, RVG-NT-3-Exo treatment alleviated the decrease in blink frequency caused by FNA (Fig. 6C). On balance, RVG-NT-3 Exo boosted myelin sheath repair after facial nerve injury.

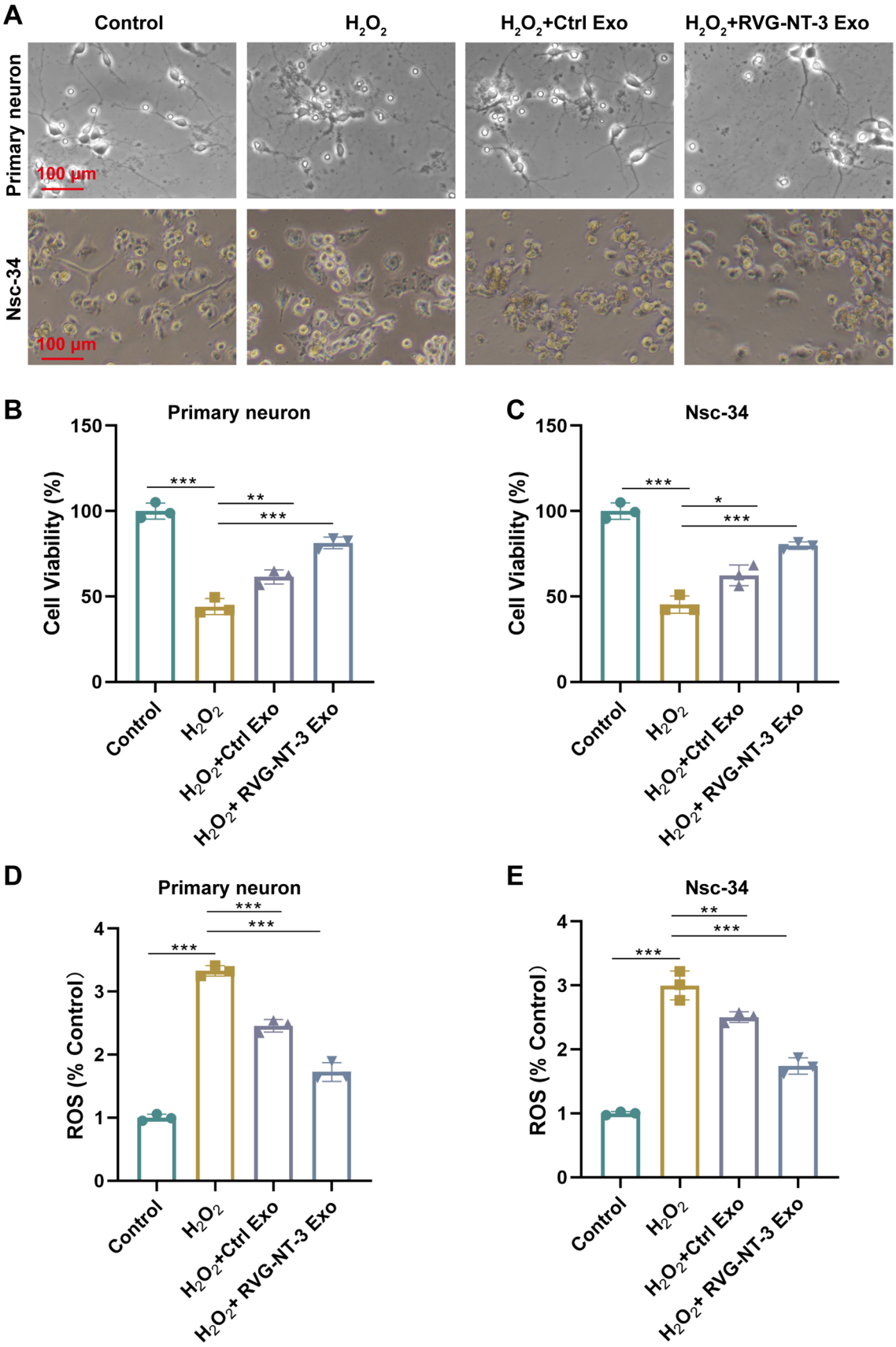
A
Control
H2O2
H2O2+Ctrl Exo
H2O2+RVG-NT-3 Exo
Primary neuron
Nsc-34
100 μm
100 μm
B
Primary neuron
Cell Viability (%)
150
100
50
0
***
**
***
Control
H2O2
H2O2+Ctrl Exo
H2O2+ RVG-NT-3 Exo
C
Nsc-34
Cell Viability (%)
150
100
50
0
***
*
***
Control
H2O2
H2O2+Ctrl Exo
H2O2+ RVG-NT-3 Exo
D
Primary neuron
ROS (% Control)
4
3
2
1
0
***
***
***
Control
H2O2
H2O2+Ctrl Exo
H2O2+ RVG-NT-3 Exo
E
Nsc-34
ROS (% Control)
4
3
2
1
0
**
***
***
Control
H2O2
H2O2+Ctrl Exo
H2O2+ RVG-NT-3 Exo

◂**Fig. 3** The protective effect of RVG-NT-3 Exo on H_2O_2-induced oxidative stress damage in neurons. **A** Morphological changes for primary neurons and Nsc-34 cells were observed using a bright-field microscope in different groups (Control, H_2O_2, H_2O_2 + Ctrl Exo, and H_2O_2 + RVG-NT-3 Exo) ($n = 3$). **B** and **C** The viability of primary neurons and Nsc-34 cells in different groups was determined by CCK-8 assays ($n = 3$). **D** and **E** Estimation of ROS production in different groups by DCFH-DA. The fluorescence intensity was normalized to the control group (% control) ($n = 3$). Statistical analysis was done by two-tailed unpaired Student's *t* test (***$p < 0.001$ vs. Control) or one-way ANOVA with multiple comparisons ($^{\#}p < 0.05$, $^{\#\#}p < 0.01$, and $^{\#\#\#}p < 0.001$ vs. H_2O_2). All quantitative data are presented as mean ± SD

Discussion

The main function of the facial nerve is to control the movement of facial muscles. The facial nerve is the 7th cranial nerve and contains three main fibrous components, most of which are motor fibers and a small part of which are parasympathetic and sensory fibers [32]. Unlike other traumas, once peripheral nerves are damaged, the connection between the center and the target organ is interrupted and difficult to recover, resulting in motor or sensory impairment of the target organ [33]. After facial nerve injury, it is extremely difficult to regenerate nerves and restore their functions, so the treatment of facial paralysis caused by facial nerve injury is difficult [34]. Therefore, the study of facial nerve repair has an important significance.

Exos are lipid bilayer membrane vesicles that are secreted by a variety of cell types and participate in cell-to-cell communication by delivering coding and non-coding RNAs, receptors, and enzymes between cells [35]. It has been reported that exos derived from MSCs do not contain human major histocompatibility complex (MHC) I and II antigens and co-stimulatory molecules such as CD80 and CD86 [36]. Exos lacking these surface proteins are suitable for allogeneic therapy without immune rejection, and long-term repeated injections of exos do not produce toxicity [37]. Increased evidence confirms the ability of exos to cross the blood–brain barrier. Therefore, exos play crucial roles in the pathologic process of the peripheral nervous system [38]. Recent research supports the role of exos in exhibiting neurotherapeutic effects through axonal growth, schwann cell activation, and regulating inflammation [39–41]. Due to the lack of modification on the membrane surface, exos do not have natural targeting, but they can bind to a range of surface adhesion proteins and specific carrier ligands (tetra transmembrane proteins, integrins, CD11b receptors, and CD18 receptors) to deliver drugs to target cells [42]. To endow the exos with the ability to specifically target neurons, researchers fused RVG that can specifically bind to AchR into Lamp2b and then engineered it onto the extracellular vesicle membrane [43]. Moreover, RVG-Lamp2b-modified exos have been studied for drug or gene delivery. For instance, RVG-Lamp2b-modified exos efficiently transferred siRNA to the central nervous system to downregulate MOR expression levels, thus mediating the treatment of morphine relapse [44]. RVG-Lamp2b-modified exos loaded with miR-25 or miR-181a reduced neuron apoptosis and induced motor improvements in SCA3 mouse models [45]. These studies have demonstrated the potential of RVG-Lamp2b-modified exos as carriers for targeting the nervous system.

NT-3, a classic trophic factor, plays a crucial role in cell survival, differentiation, and axonal growth in the peripheral nervous system [46]. NT-3 can bind to tyrosine kinase receptors present on cells throughout the peripheral nervous system, thereby mediating neuronal cell migration, myelination formation, and axon growth and improved sensory axon regeneration [47–49]. The use of NT-3 as a clinical therapeutic drug is limited by its short half-life, so the delivery of NT-3 through biomaterials is of interest and exploration [14]. Li et al. declared that transplantation of a NT-3/fibroin-coated gelatin sponge scaffold to the spinal cord injury site in rats could promote tissue regeneration and axonal extension related to the myelin sheath, leading to a significant reduction in the cavity area of the injury site [15]. The electrospun fiber-mediated delivery of NT-3 elevated the ability of Schwann cells and accelerated the axonal growth of the dorsal root ganglion [10]. Adipose-derived stem cell-derived exos encapsulated NT-3 were loaded into alginate hydrogel, and this platform could promote nerve regeneration and improve the functional recovery of gastrocnemius muscles [50]. Genetic engineering technology is the most common method endowing exos with stronger targeting properties by making recipient cells highly express targeting proteins or polypeptides, thereby secreting target-specific exos [51]. Besides, it's also an accepted approach to package biological molecules into secreted exos [52]. In this study, we co-transfected RVG-Lamp2b and NT-3 plasmids into bone marrow MSCs and then obtained RVG-NT-3 Exo by gradient centrifugation. As a result, Lamp2b and NT-3 proteins were more abundant in RVG-NT-3 Exo than Ctrl Exo, which indicated that Lamp2b and NT-3 proteins were successfully incorporated into RVG-NT-3 Exo. Through characterization experiments, it was found that there was no significant difference between RVG-NT-3 Exo and Ctrl Exo, indicating that loading NT-3 and modifying with RVG-Lamp2b did not alter the properties of the exos, including morphology, particle size distribution, and size distribution or protein marker expression. Unlike biochemical methods, genetic engineering technology incorporates target substances in the process of exosomal biogenesis hence without causing damage to exosome membrane proteins [53]. In addition to primary neurons, our study also included NSC-34 motorneuron-like cells for further in vitro analysis, an accepted model for studying the pathophysiology of motorneurons, which share numerous morphological and physiological characteristics with mature

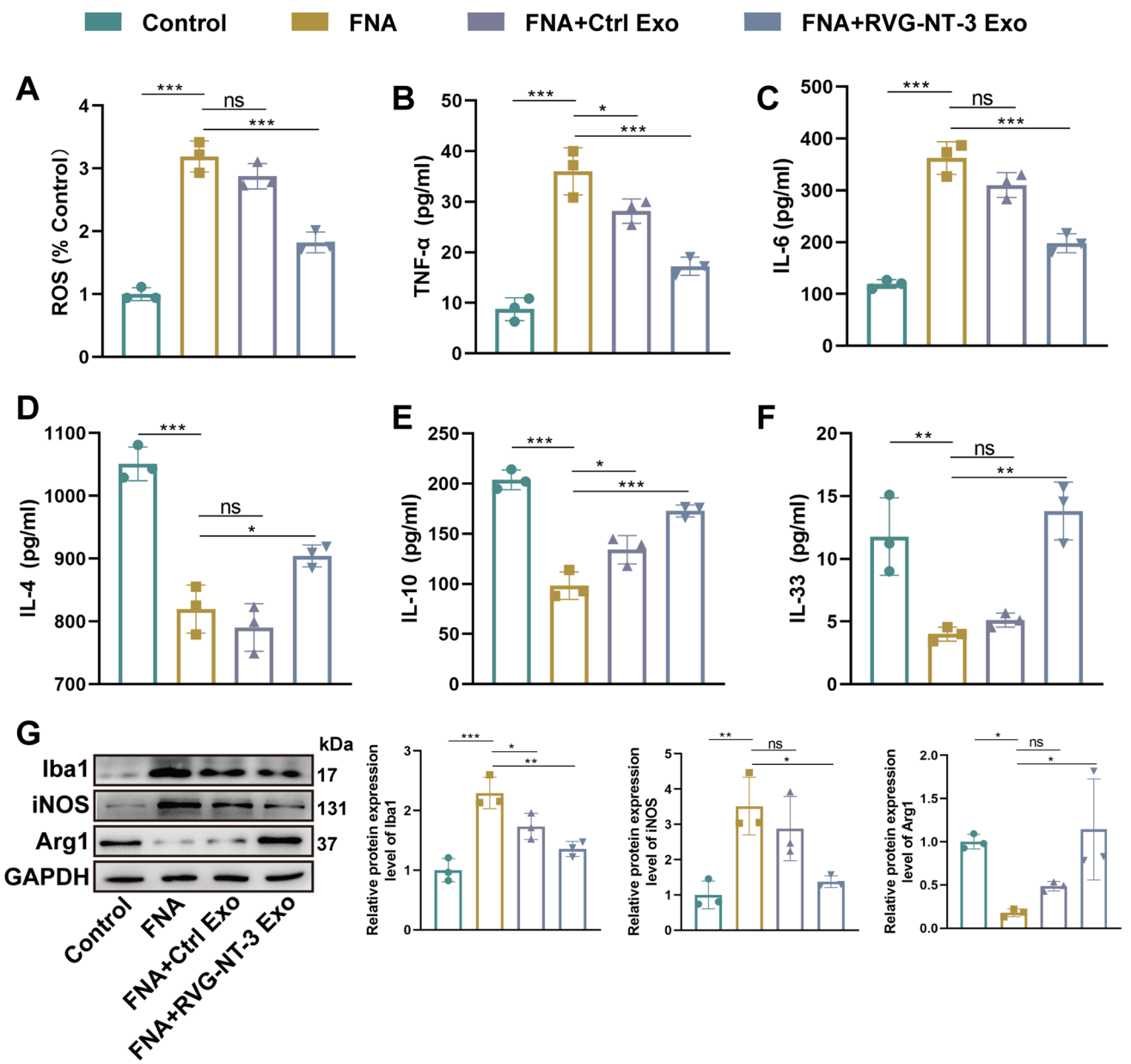

Fig. 4 RVG-NT-3 Exo overtly lowered FNA-induced inflammation. **A** The production of ROS in facial nerve samples of different groups (Control, FNA, FNA + Ctrl-Exo, or FNA + RVG-NT-3-Exo) was detected by DCFH-DA ($n = 5$). **B**–**F** ELISA analysis of the release of inflammatory cytokines TNF-α (**B**), IL-6 (**C**), IL-4 (**D**), IL-10 (**D**), and IL-33 (**E**) ($n = 5$). **G** Microglial activation and polarization markers Iba1, iNOS, and Arg1 in facial nerve samples were detected by western blotting ($n = 5$). Statistical analysis was done by two-tailed unpaired Student's *t*-test (*$p < 0.05$, **$p < 0.01$, and ***$p < 0.001$ vs. Control) or one-way ANOVA with multiple comparisons (*$p < 0.05$, **$p < 0.01$, and ***$p < 0.001$ vs. FNA). *ns* no significance. All quantitative data are presented as mean ± SD

primary motorneurons [54]. After co-incubation with RVG-NT-3 Exo, NT-3 mRNA levels in primary neurons and Nsc-34 cells were higher than before incubation, indicating that RVG-NT-3 Exo could target neurons for NT-3 delivery.

Oxidative stress damage is a common pathological mechanism in various neurodegenerative diseases [55], and it is closely related to abnormal nerve fiber tangles, neuroinflammatory reactions, and neuronal apoptosis [56, 57]. ROS can not only affect the neurophysiological processes such as synaptic plasticity and neurotransmitter release of neurons [58, 59], but also act on biological macromolecules such as cell membrane structure, protein, and nucleic acid, causing peroxidation damage, even neuronal death [60]. ROS is one of the contributors to the pathogenesis of facial nerve injury [61], which causes cellular damage through oxidative stress. Thus, inhibiting

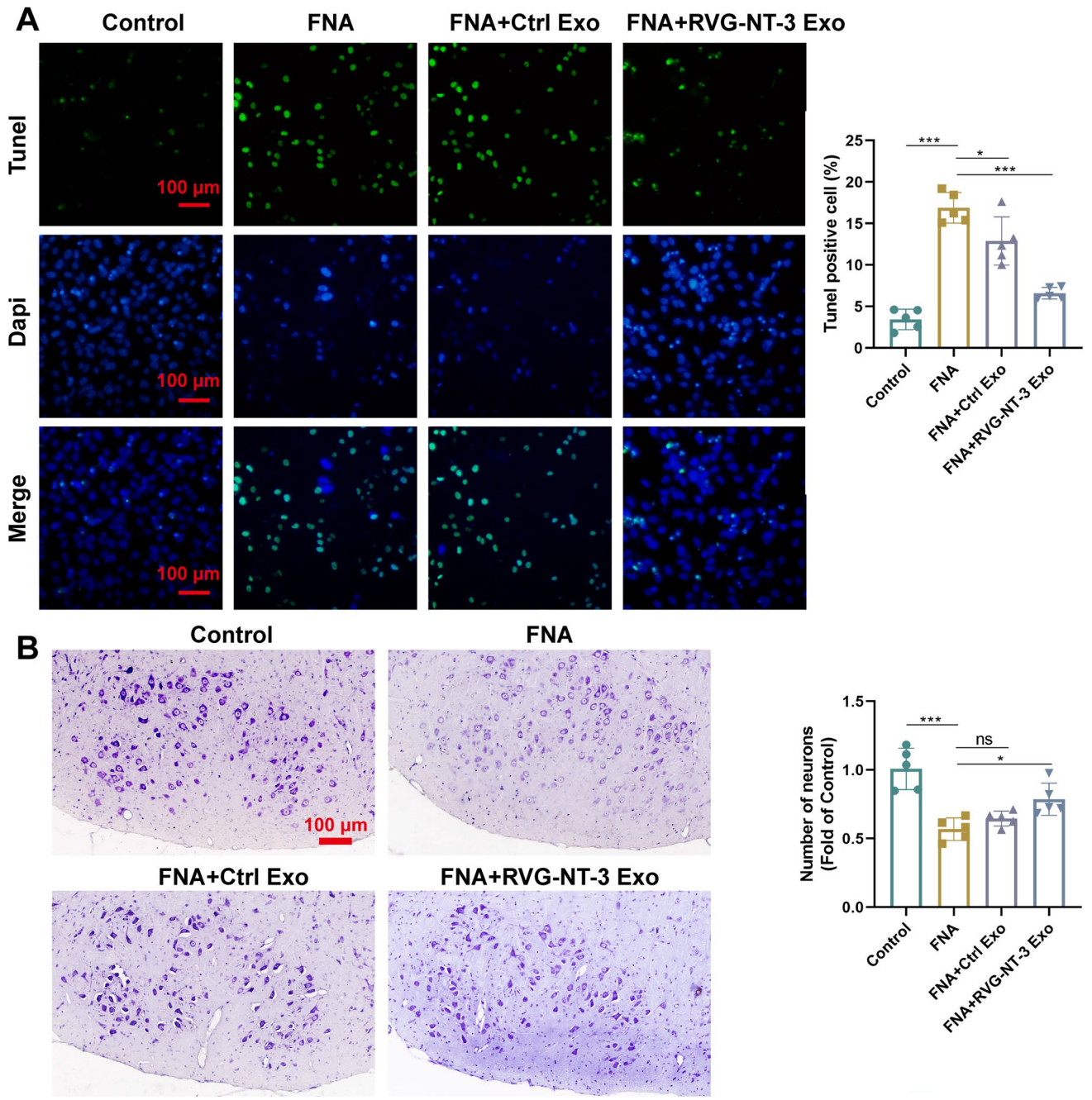

Fig. 5 RVG-NT-3 Exo lightened FNA-induced neuron apoptosis and FMN death. **A** Tunel staining analysis of neuron apoptosis in facial nerve samples in different groups (Control, FNA, FNA + Ctrl-Exo, or FNA + RVG-NT-3-Exo) ($n = 5$). **B** Changes of Nissl bodies in facial nerve samples were determined by Nissl staining ($n = 5$). Statistical analysis was done by two-tailed unpaired Student's *t* test (**$p < 0.01$ and ***$p < 0.001$ vs. Control) or one-way ANOVA with multiple comparisons (*$p < 0.05$ and **$p < 0.01$ vs. FNA). *ns* no significance. All quantitative data are presented as mean ± SD

ROS production could mitigate oxidative damage induced by facial nerve injury. Exposure of primary neurons and Nsc-34 cells to H_2O_2 was used to observe the protection of RVG-NT-3 Exo on ROS-induced neuron damage *in vitro*. Herein, RVG-NT-3 Exo treatment alleviated H_2O_2-mediated synaptic loss and cell contraction in primary neurons and Nsc-34 cells compared to Ctrl Exo. Furthermore, RVG-NT-3 Exo treatment impaired H_2O_2 stimulation-mediated decreased viability and increased ROS production in primary neurons and Nsc-34 cells. These data suggested that RVG-NT-3 Exo could effectively alleviate H_2O_2-induced neuronal oxidative stress damage.

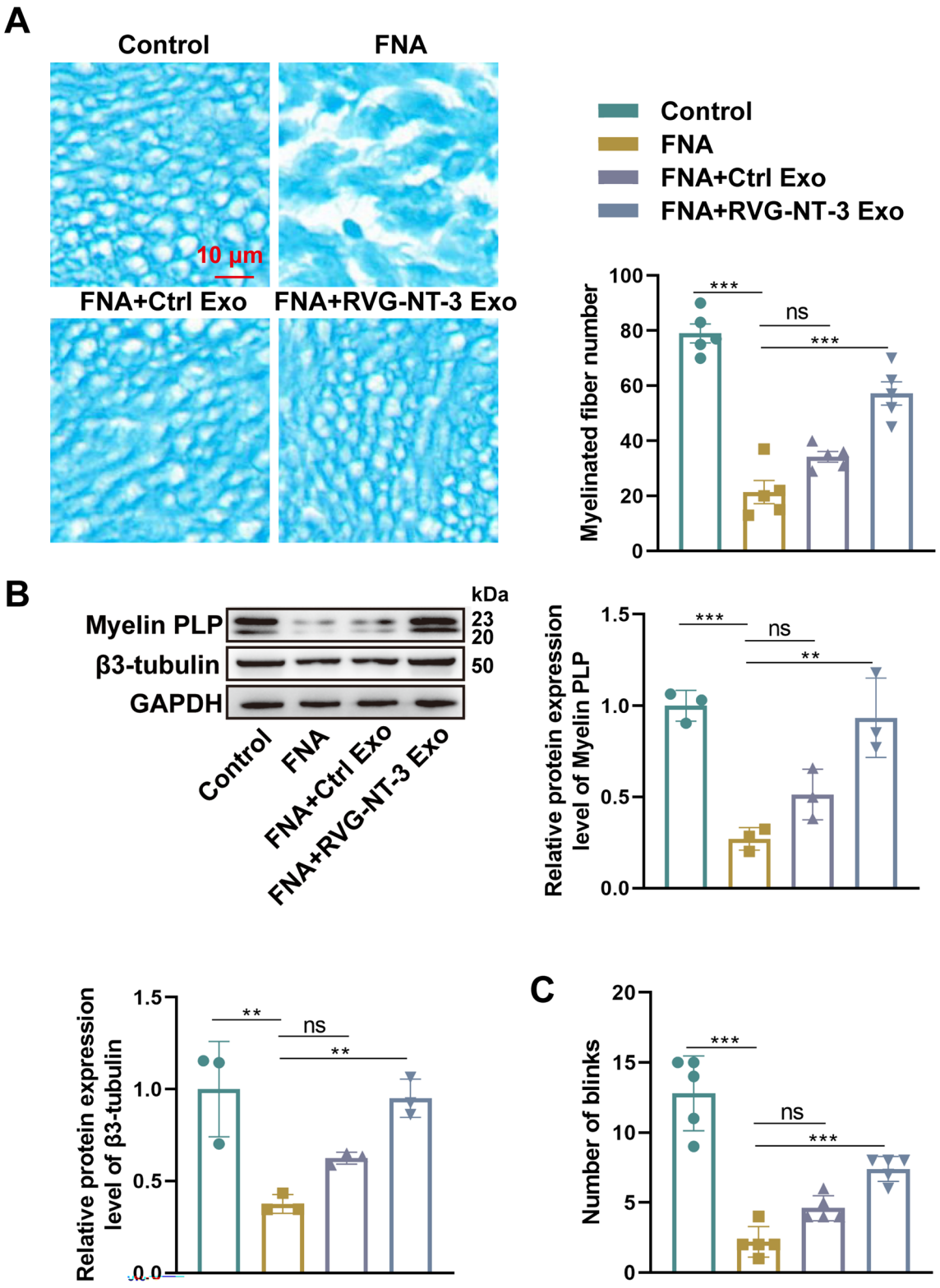

Fig. 6 RVG-NT-3 Exo intensified myelin sheath repair after facial nerve injury. **A** LFB staining analysis of the morphology, structure, and pathological changes of the myelin sheath in facial nerve samples ($n=5$). **B** Detection of myelin PLP and β3-tubulin proteins associated with myelin sheath in facial nerve samples ($n=5$). (**C**) The number of blinks in different groups of rats on the injured side ($n=5$). Statistical analysis was done by two-tailed unpaired Student's *t*-test (***$p<0.001$ vs. Control) or one-way ANOVA with multiple comparisons (*$p<0.05$, **$p<0.01$, and ***$p<0.001$ vs. FNA). *ns* no significance. All data are presented as mean ± SD

The facial nerve is a peripheral nerve that is an important nerve of the cranial face, with a superficial anatomical position and a complex anatomical structure. Damage and regeneration of peripheral nerves is a complex process that includes the survival of axon-breaking neurons, the regeneration of a sufficient number of nerve axons, accurate reinnervation of target organs, and reconstruction of functional synaptic connections [62, 63]. The disconnection of the axon means that a certain volume of the cytosol is cut off on the neuronal cell body, resulting in significant changes in the function of the cell structure and even causing cell death [64]. Axon disconnection also triggers a programmed apoptosis response in FMNs [65, 66]. Microglia in the facial nerve nucleus plays an important role in the central immunomodulatory and inflammatory response triggered by axon disconnection, thereby affecting FMN survival and axon regeneration [67, 68]. Microglia in the peripheral nervous system are distributed along neuronal axons and wrapped around nerve fibers to form myelinated nerve fibers [69, 70]. Once peripheral nerve damage occurs, microglial cells can secrete a large amount of NT-3, promote the survival of damaged neurons and the regeneration of axons, and participate in the formation of nerve fibers in the peripheral nervous system [71, 72]. Microglia also promote the survival of damaged neurons, guide and support axon regeneration [73], secrete neurotrophins [74], and regenerate myelin sheaths [75].

Due to the advantages of simplicity, reproducibility, interspecies consistency, reliable survival rates, and an increased anatomic size relative to murine models, the FNA rat model was the most widely used for studying nerve regeneration [76]. In this study, we constructed FNA rat models to explore the function of RVG-NT-3 Exo. Since the important precursors to facial nerve injury, such as Nissl body dissolution and facial neuron apoptosis, were usually observed on 7 days after surgery [77, 78], the administration was also performed on day 7 except for day 0. The results showed that RVG-NT-3 Exo treatment significantly reduced ROS production and release of pro-inflammatory cytokines TNF-α and IL-6, as well as increased release of anti-inflammatory cytokines IL-4, IL-10 and IL-33, suggesting that RVG-NT-3 Exo treatment reduced inflammatory and oxidative stress in FNA rat models. RVG-NT-3-Exo treatment lowered Iba1 and iNOS protein levels, as well as increased Arg1 protein levels, indicating that RVG-NT-3-Exo treatment promoted the polarization of microglia to the anti-inflammatory phenotype. RVG-NT-3 Exo treatment lowered the elevated number of Tunel-positive cells mediated by FNA. RVG-NT-3 Exo treatment improved FNA-mediated reduction in the number of motor neurons, manifesting that RVG-NT-3 Exo reduced FNA-induced apoptosis and facial motor neuron death. RVG-NT-3-Exo treatment partially elevated the number of myelinated nerve fibers and Myelin PLP and β3-tubulin protein levels, suggesting that RVG-NT-3 Exo boosts myelin repair after facial nerve injury. Thus, our animal studies showed that this nanoplatform (RVG-NT-3 Exo) has the potential to penetrate facial nerves and promote axonal, FMN, and myelin regeneration.

However, there were a few methodological limitations in this study. Our animal experiments only used male rats. It has reported the sex-specific differences in the actions of gonadal hormones on central and peripheral glia [79]. For example, estradiol and progesterone regulate Schwann cell proliferation in the peripheral nervous system, which is essential for the maintenance, regeneration, and remyelination of peripheral nerves; but this effect was only observed in the peripheral nerves of males [80]. Hence, further studies are required to be performed on female rats to validate the neuroprotective effects of RVG-NT-3 Exo. The present study only focuses on the immediate and short-term therapeutic effects of RVG-NT-3 Exo, lacking an investigation of its long-term outcomes and functional recovery, and a deeper exploration into the post-delivery mechanisms, which will be the important direction of our future research. Moreover, to better position RVG-NT-3 Exo within the existing treatment landscape, a comparative analysis comparing the efficacy of RVG-NT-3 Exo treatment directly with the standard therapies is required. Besides, since the potential of modifications with RVG-Lamp2b and NT-3 altering the immunogenic profile of MSC-derived exos, the immunogenicity, biodistribution, pharmacokinetics, and safety of RVG-NT-3 Exo need to be further explored before the clinical application. Lastly, to accelerate the clinical translation of these findings, designing manufacturing strategies for producing clinical-grade and large-scale exos and determining minimal effective dose and route of delivery for clinical trials is another important future research mission.

In summary, we designed an engineered exo-based therapeutic platform targeting neurons and delivering NT-3. The results showed that engineered RVG-NT-3 Exo could reduce oxidative stress damage, neuroinflammatory response, facial motor neuron death, and boosted microglia activation and myelin sheath repair. Our work can provide new strategies for the treatment of facial nerve injury, hoping to broaden the prospects for accurate diagnosis and treatment of facial nerve injury in the future.

Supplementary Information The online version contains supplementary material available at https://doi.org/10.1007/s13577-024-01086-7.

Acknowledgements None.

Funding This work was supported by the Major State Basic Research Development Program of China (grant number 2017YFA0104703) and National Natural Science Foundation of China (grant number 81901023).

Data availability The data that support the findings of this study are available from the corresponding author upon reasonable request.

Declarations

Conflicts of interest The authors declare that there is no conflict of interest.

Ethics approval This study was performed followed the Guide for the Care and Use of Laboratory Animals after being approved by the First Medical Center, Chinese PLA General Hospital Animal Care and Use Committee (Approval number SQ2022401).

Informed consent Not applicable.

References

1. Schroeter F, Amyai N, Petignat PA, Wicki B. Facial palsy: diagnostic traps. Revue medicale suisse. 2023;19(836):1413–8. https://doi.org/10.53738/revmed.2023.19.836.1413.
2. Kinoshita I, Kawata R, Higashino M, Terada T, Haginomori SI, Tochizawa T. Tumor localization is the important factor for recovery time of postoperative facial nerve paralysis in benign parotid surgery. Auris Nasus Larynx. 2023;51(1):214–20. https://doi.org/10.1016/j.anl.2023.07.002.
3. Zhou Y, Dong X, Xing Y, Wang R, Yang S, Han Y, et al. Effects of electroacupuncture therapy on intractable facial paralysis: a systematic review and meta-analysis. PLoS ONE. 2023. https://doi.org/10.1371/journal.pone.0288606.
4. Tawfik HA, Dutton JJ. Facial nerve palsy and the eye: etiology, diagnosis, and management. Int Ophthalmol Clin. 2023;63(3):75–94. https://doi.org/10.1097/iio.0000000000000457.
5. Lee JM, Choi YJ, Yoo MC, Yeo SG. Central facial nervous system biomolecules involved in peripheral facial nerve injury responses and potential therapeutic strategies. Antioxidants (Basel, Switzerland). 2023;12(5):1036. https://doi.org/10.3390/antiox12051036.
6. Shekari A, Fahnestock M. Retrograde axonal transport of neurotrophins in basal forebrain cholinergic neurons. Methods Mol Biol (Clifton, NJ). 2022;2431:249–70. https://doi.org/10.1007/978-1-0716-1990-2_13.
7. Yamashita N. Retrograde signaling via axonal transport through signaling endosomes. J Pharmacol Sci. 2019;141(2):91–6. https://doi.org/10.1016/j.jphs.2019.10.001.
8. Hernández-Echeagaray E. Neurotrophin-3 modulates synaptic transmission. Vitam Horm. 2020;114:71–89. https://doi.org/10.1016/bs.vh.2020.04.008.
9. Rocco ML, Soligo M, Manni L, Aloe L. Nerve growth factor: early studies and recent clinical trials. Curr Neuropharmacol. 2018;16(10):1455–65. https://doi.org/10.2174/1570159x16666180412092859.
10. Puhl DL, Funnell JL, Fink TD, Swaminathan A, Oudega M, Zha RH, et al. Electrospun fiber-mediated delivery of neurotrophin-3 mRNA for neural tissue engineering applications. Acta Biomater. 2023;155:370–85. https://doi.org/10.1016/j.actbio.2022.11.025.
11. Wang XY, Gu PY, Chen SW, Gao WW, Tian HL, Lu XH, et al. Endogenous neurotrophin-3 promotes neuronal sprouting from dorsal root ganglia. Neural Regen Res. 2015;10(11):1865–8. https://doi.org/10.4103/1673-5374.170318.
12. Wan H, Zhang L, Blanchard S, Bigou S, Bohl D, Wang C, et al. Combination of hypoglossal-facial nerve surgical reconstruction and neurotrophin-3 gene therapy for facial palsy. J Neurosurg. 2013;119(3):739–50. https://doi.org/10.3171/2013.1.Jns121176.
13. Wang H, Ni H, Han S, Xu W, Wang J, Yuan B, et al. The promotion of neural regeneration in A Rat facial nerve crush injury model using collagen-binding NT-3. Ann Clin Lab Sci. 2016;46(6):578–85.
14. Sahenk Z, Galloway G, Clark KR, Malik V, Rodino-Klapac LR, Kaspar BK, et al. AAV1NT-3 gene therapy for charcot-marie-tooth neuropathy. Mol Therapy J Am Soc Gene Therapy. 2014;22(3):511–21. https://doi.org/10.1038/mt.2013.250.
15. Li G, Che MT, Zhang K, Qin LN, Zhang YT, Chen RQ, et al. Graft of the NT-3 persistent delivery gelatin sponge scaffold promotes axon regeneration, attenuates inflammation, and induces cell migration in rat and canine with spinal cord injury. Biomaterials. 2016;83:233–48. https://doi.org/10.1016/j.biomaterials.2015.11.059.
16. Yao S, Rong W, Yuan Y. Optimization of adeno-associated virus (AAV) gene delivery into human bone marrow stem cells (hBMSCs). Stem Cell Investig. 2023;10:3. https://doi.org/10.21037/sci-2022-042.
17. Kalluri R, LeBleu VS. The biology, function, and biomedical applications of exosomes. Science (New York, NY). 2020;367(6478):eaau6977. https://doi.org/10.1126/science.aau6977.
18. Kimiz-Gebologlu I, Oncel SS. Exosomes: Large-scale production, isolation, drug loading efficiency, and biodistribution and uptake. J Contr Release Off J Contr Rel Soc. 2022;347:533–43. https://doi.org/10.1016/j.jconrel.2022.05.027.
19. Tenchov R, Sasso JM, Wang X, Liaw WS, Chen CA, Zhou QA. Exosomes─nature's lipid nanoparticles, a rising star in drug delivery and diagnostics. ACS Nano. 2022;16(11):17802–46. https://doi.org/10.1021/acsnano.2c08774.
20. Szabłowska-Gadomska I, Rudziński S, Dymowska M. Secretome of mesenchymal stromal cells as a possible innovative therapeutic tool in facial nerve injury treatment. Biomed Res Int. 2023;2023:8427200. https://doi.org/10.1155/2023/8427200.
21. Liang Y, Duan L, Lu J, Xia J. Engineering exosomes for targeted drug delivery. Theranostics. 2021;11(7):3183–95. https://doi.org/10.7150/thno.52570.
22. Ma J, Zhao Y, Sun L, Sun X, Zhao X, Sun X, et al. Exosomes derived from akt-modified human umbilical cord mesenchymal stem cells improve cardiac regeneration and promote angiogenesis via activating platelet-derived growth factor D. Stem Cells Transl Med. 2017;6(1):51–9. https://doi.org/10.5966/sctm.2016-0038.
23. Tamura R, Uemoto S, Tabata Y. mented liver targeting of exosomes by surface modification with cationized pullulan. Acta Biomater. 2017;57:274–84. https://doi.org/10.1016/j.actbio.2017.05.013.
24. Bauer A, Nolden T, Schröter J, Römer-Oberdörfer A, Gluska S, Perlson E, et al. Anterograde glycoprotein-dependent transport of newly generated rabies virus in dorsal root ganglion neurons. J Virol. 2014;88(24):14172–83. https://doi.org/10.1128/jvi.02254-14.
25. Yang J, Zhang X, Chen X, Wang L, Yang G. Exosome mediated delivery of miR-124 promotes neurogenesis after ischemia. Mol Therapy Nuc Acids. 2017;7:278–87. https://doi.org/10.1016/j.omtn.2017.04.010.
26. Lai N, Wu D, Liang T, Pan P, Yuan G, Li X, et al. Systemic exosomal miR-193b-3p delivery attenuates neuroinflammation in early brain injury after subarachnoid hemorrhage in mice. J Neuroinflammation. 2020;17(1):74. https://doi.org/10.1186/s12974-020-01745-0.
27. Sango K. el neuron-Schwann cell co-culture models to study peripheral nerve degeneration and regeneration. Neural Regen Res. 2023;18(8):1732–3. https://doi.org/10.4103/1673-5374.363195.
28. Zhang Y, Liu J, Su M, Wang X, Xie C. Exosomal microRNA-22-3p alleviates cerebral ischemic injury by modulating KDM6B/

BMP2/BMF axis. Stem Cell Res Ther. 2021;12(1):111. https://doi.org/10.1186/s13287-020-02091-x.
29. Zhang R, Fu Y, Cheng M, Ma W, Zheng N, Wang Y, et al. sEVs(RVG) selectively delivers antiviral siRNA to fetus brain, inhibits ZIKV infection and mitigates ZIKV-induced microcephaly in mouse model. Mol Therapy J Am Soc Gene Therapy. 2022;30(5):2078–91. https://doi.org/10.1016/j.ymthe.2021.10.009.
30. Pfaffl MW. A new mathematical model for relative quantification in real-time RT-PCR. Nucleic Acids Res. 2001. https://doi.org/10.1093/nar/29.9.e45.
31. Liu Z, Yan M, Lei W, Jiang R, Dai W, Chen J, et al. Sec13 promotes oligodendrocyte differentiation and myelin repair through autocrine pleiotrophin signaling. J Clin Investig. 2022. https://doi.org/10.1172/jci155096.
32. Yang SH, Park H, Yoo DS, Joo W, Rhoton A. Microsurgical anatomy of the facial nerve. Clin Anat (New York, NY). 2021;34(1):90–102. https://doi.org/10.1002/ca.23652.
33. Ottaiano AC, Gomez GD, Freddi TAL. The facial nerve: anatomy and pathology. Semin Ultrasound CT MR. 2023;44(2):71–80. https://doi.org/10.1053/j.sult.2022.11.005.
34. Bengur FB, Stoy C, Binko MA, Nerone WV, Fedor CN, Solari MG, et al. Facial nerve repair: bioengineering approaches in preclinical models. Tissue Eng Part B Rev. 2022;28(2):364–78. https://doi.org/10.1089/ten.TEB.2020.0381.
35. Mathieu M, Martin-Jaular L, Lavieu G, Théry C. Specificities of secretion and uptake of exosomes and other extracellular vesicles for cell-to-cell communication. Nat Cell Biol. 2019;21(1):9–17. https://doi.org/10.1038/s41556-018-0250-9.
36. Marofi F, Alexandrovna KI, Margiana R, Bahramali M, Suksatan W, Abdelbasset WK, et al. MSCs and their exosomes: a rapidly evolving approach in the context of cutaneous wounds therapy. Stem Cell Res Ther. 2021;12(1):597. https://doi.org/10.1186/s13287-021-02662-6.
37. Sareen N, Srivastava A, Alagarsamy KN, Lionetti V, Dhingra S. Stem cells derived exosomes and biomaterials to modulate autophagy and mend broken hearts. Biochim Biophys Acta. 2023. https://doi.org/10.1016/j.bbadis.2023.166806.
38. Supra R, Wilson DR, Agrawal DK. Therapeutic potential of "smart" exosomes in peripheral nerve regeneration. J Biotechnol Biomed. 2023;6(2):189–96. https://doi.org/10.26502/jbb.2642-91280082.
39. Zhang Y, Chopp M, Meng Y, Katakowski M, Xin H, Mahmood A, et al. Effect of exosomes derived from multipluripotent mesenchymal stromal cells on functional recovery and neurovascular plasticity in rats after traumatic brain injury. J Neurosurg. 2015;122(4):856–67. https://doi.org/10.3171/2014.11.Jns14770.
40. Bucan V, Vaslaitis D, Peck CT, Strauß S, Vogt PM, Radtke C. Effect of exosomes from rat adipose-derived mesenchymal stem cells on neurite outgrowth and sciatic nerve regeneration after crush injury. Mol Neurobiol. 2019;56(3):1812–24. https://doi.org/10.1007/s12035-018-1172-z.
41. Yin G, Yu B, Liu C, Lin Y, Xie Z, Hu Y, et al. Exosomes produced by adipose-derived stem cells inhibit schwann cells autophagy and promote the regeneration of the myelin sheath. Int J Biochem Cell Biol. 2021;132: 105921. https://doi.org/10.1016/j.biocel.2021.105921.
42. Sun C, Qin Y, Zhuang H, Zhang Y, Wu Z, Chen Y. Membrane vesicles as drug delivery systems: source, preparation, modification, drug loading, in vivo administration and biodistribution, and application in various diseases. Pharmaceutics. 2023;15(7):1903. https://doi.org/10.3390/pharmaceutics15071903.
43. Alvarez-Erviti L, Seow Y, Yin H, Betts C, Lakhal S, Wood MJ. Delivery of siRNA to the mouse brain by systemic injection of targeted exosomes. Nat Biotechnol. 2011;29(4):341–5. https://doi.org/10.1038/nbt.1807.
44. Liu Y, Li D, Liu Z, Zhou Y, Chu D, Li X, et al. Targeted exosome-mediated delivery of opioid receptor Mu siRNA for the treatment of morphine relapse. Sci Rep. 2015;5:17543. https://doi.org/10.1038/srep17543.
45. Tang Z, Hu S, Wu Z, He M. Therapeutic effects of engineered exosome-based miR-25 and miR-181a treatment in spinocerebellar ataxia type 3 mice by silencing ATXN3. Mol Med Cambridge Mass). 2023;29(1):96. https://doi.org/10.1186/s10020-023-00695-6.
46. Ulrichsen M, Gonçalves NP, Mohseni S, Hjæresen S, Lisle TL, Molgaard S, et al. Sortilin modulates schwann cell signaling and remak bundle regeneration following nerve injury. Front Cell Neurosci. 2022. https://doi.org/10.3389/fncel.2022.856734.
47. Akyol O, Sherchan P, Yilmaz G, Reis C, Ho WM, Wang Y, et al. Neurotrophin-3 provides neuroprotection via TrkC receptor dependent pErk5 activation in a rat surgical brain injury model. Exp Neurol. 2018;307:82–9. https://doi.org/10.1016/j.expneurol.2018.06.002.
48. Cui Y, Yin Y, Zou Y, Zhao Y, Han J, Xu B, et al. The rotary cell culture system increases NTRK3 expression and promotes neuronal differentiation and migratory ability of neural stem cells cultured on collagen sponge. Stem Cell Res Ther. 2021;12(1):298. https://doi.org/10.1186/s13287-021-02381-y.
49. Ménard M, Costechareyre C, Coelho-Aguiar JM, Jarrosson-Wuilleme L, Rama N, Blachier J, et al. The dependence receptor TrkC regulates the number of sensory neurons during DRG development. Dev Biol. 2018;442(2):249–61. https://doi.org/10.1016/j.ydbio.2018.07.022.
50. Yang Z, Yang Y, Xu Y, Jiang W, Shao Y, Xing J, et al. Biomimetic nerve guidance conduit containing engineered exosomes of adipose-derived stem cells promotes peripheral nerve regeneration. Stem Cell Res Ther. 2021;12(1):442. https://doi.org/10.1186/s13287-021-02528-x.
51. Xu M, Feng T, Liu B, Qiu F, Xu Y, Zhao Y, et al. Engineered exosomes: desirable target-tracking characteristics for cerebrovascular and neurodegenerative disease therapies. Theranostics. 2021;11(18):8926–44. https://doi.org/10.7150/thno.62330.
52. Amiri A, Bagherifar R, Ansari Dezfouli E, Kiaie SH, Jafari R, Ramezani R. Exosomes as bio-inspired nanocarriers for RNA delivery: preparation and applications. J Transl Med. 2022;20(1):125. https://doi.org/10.1186/s12967-022-03325-7.
53. Huang L, Wu E, Liao J, Wei Z, Wang J, Chen Z. Research advances of engineered exosomes as drug delivery carrier. ACS Omega. 2023;8(46):43374–87. https://doi.org/10.1021/acsomega.3c04479.
54. Cashman NR, Durham HD, Blusztajn JK, Oda K, Tabira T, Shaw IT, et al. Neuroblastoma x spinal cord (NSC) hybrid cell lines resemble developing motor neurons. Dev Dyn. 1992;194(3):209–21. https://doi.org/10.1002/aja.1001940306.
55. Guo C, Sun L, Chen X, Zhang D. Oxidative stress, mitochondrial damage and neurodegenerative diseases. Neural Regen Res. 2013;8(21):2003–14. https://doi.org/10.3969/j.issn.1673-5374.2013.21.009.
56. Yang T, Xu Z, Liu W, Xu B, Deng Y. Oxidative stress accelerates synaptic glutamate dyshomeostasis and NMDARs disorder during methylmercury-induced neuronal apoptosis in rat cerebral cortex. Environ Toxicol. 2020;35(6):683–96. https://doi.org/10.1002/tox.22904.
57. Teleanu DM, Niculescu AG, Lungu II, Radu CI, Vladâcenco O, Roza E, et al. An overview of oxidative stress, neuroinflammation, and neurodegenerative diseases. Int J Mol Sci. 2022;23(11):5938. https://doi.org/10.3390/ijms23115938.
58. Wang P, Wang F, Ni L, Wu P, Chen J. Targeting redox-altered plasticity to reactivate synaptic function: a novel therapeutic strategy for cognitive disorder. Acta pharmaceutica Sinica B. 2021;11(3):599–608. https://doi.org/10.1016/j.apsb.2020.11.012.

59. Flippo KH, Strack S. Mitochondrial dynamics in neuronal injury, development and plasticity. J Cell Sci. 2017;130(4):671–81. https://doi.org/10.1242/jcs.171017.
60. Navarro-Yepes J, Zavala-Flores L, Anandhan A, Wang F, Skotak M, Chandra N, et al. Antioxidant gene therapy against neuronal cell death. Pharmacol Ther. 2014;142(2):206–30. https://doi.org/10.1016/j.pharmthera.2013.12.007.
61. Phaniendra A, Jestadi DB, Periyasamy L. Free radicals: properties, sources, targets, and their implication in various diseases. Indian J Clin Biochem. 2015;30(1):11–26. https://doi.org/10.1007/s12291-014-0446-0.
62. Poitras T, Zochodne DW. Unleashing intrinsic growth pathways in regenerating peripheral neurons. Int J Mol Sci. 2022;23(21):13566. https://doi.org/10.3390/ijms232113566.
63. Klimovich P, Rubina K, Sysoeva V, Semina E. New frontiers in peripheral nerve regeneration: concerns and remedies. Int J Mol Sci. 2021;22(24):13380. https://doi.org/10.3390/ijms222413380.
64. Hussain G, Wang J, Rasul A, Anwar H, Qasim M, Zafar S, et al. Current status of therapeutic approaches against peripheral nerve injuries: a detailed story from injury to recovery. Int J Biol Sci. 2020;16(1):116–34. https://doi.org/10.7150/ijbs.35653.
65. Kim J, Kobayashi S, Shimizu-Okabe C, Okabe A, Moon C, Shin T, et al. Changes in the expression and localization of signaling molecules in mouse facial motor neurons during regeneration of facial nerves. J Chem Neuroanat. 2018;88:13–21. https://doi.org/10.1016/j.jchemneu.2017.11.002.
66. Wainwright DA, Xin J, Mesnard NA, Beahrs TR, Politis CM, Sanders VM, et al. Exacerbation of facial motoneuron loss after facial nerve axotomy in CCR3-deficient mice. ASN Neuro. 2009. https://doi.org/10.1042/an20090017.
67. Kunihiro J, Nabeka H, Wakisaka H, Unuma K, Khan MSI, Shimokawa T, et al. Prosaposin and its receptors GRP37 and GPR37L1 show increased immunoreactivity in the facial nucleus following facial nerve transection. PLoS ONE. 2020. https://doi.org/10.1371/journal.pone.0241315.
68. Mattsson P, Delfani K, Janson AM, Svensson M. Motor neuronal and glial apoptosis in the adult facial nucleus after intracranial nerve transection. J Neurosurg. 2006;104(3):411–8. https://doi.org/10.3171/jns.2006.104.3.411.
69. Hughes AN, Appel B. Microglia phagocytose myelin sheaths to modify developmental myelination. Nat Neurosci. 2020;23(9):1055–66. https://doi.org/10.1038/s41593-020-0654-2.
70. Maeda M, Tsuda M, Tozaki-Saitoh H, Inoue K, Kiyama H. Nerve injury-activated microglia engulf myelinated axons in a P2Y12 signaling-dependent manner in the dorsal horn. Glia. 2010;58(15):1838–46. https://doi.org/10.1002/glia.21053.
71. Nakajima K, Kikuchi Y, Ikoma E, Honda S, Ishikawa M, Liu Y, et al. Neurotrophins regulate the function of cultured microglia. Glia. 1998;24(3):272–89.
72. Santos E, Monzón-Mayor M, Romero-Alemán MM, Yanes C. Distribution of neurotrophin-3 during the ontogeny and regeneration of the lizard (Gallotia galloti) visual system. Dev Neurobiol. 2008;68(1):31–44. https://doi.org/10.1002/dneu.20566.
73. Ronzano R, Roux T, Thetiot M, Aigrot MS, Richard L, Lejeune FX, et al. Microglia-neuron interaction at nodes of Ranvier depends on neuronal activity through potassium release and contributes to remyelination. Nat Commun. 2021;12(1):5219. https://doi.org/10.1038/s41467-021-25486-7.
74. Nakajima K, Honda S, Tohyama Y, Imai Y, Kohsaka S, Kurihara T. Neurotrophin secretion from cultured microglia. J Neurosci Res. 2001;65(4):322–31. https://doi.org/10.1002/jnr.1157.
75. McNamara NB, Munro DAD, Bestard-Cuche N, Uyeda A, Bogie JFJ, Hoffmann A, et al. Microglia regulate central nervous system myelin growth and integrity. Nature. 2023;613(7942):120–9. https://doi.org/10.1038/s41586-022-05534-y.
76. Ali SA, Stebbins AW, Hanks JE, Kupfer RA, Hogikyan ND, Feldman EL, et al. Facial nerve surgery in the rat model to study axonal inhibition and regeneration. J Vis Exp. 2020. https://doi.org/10.3791/59224.
77. Sun Z, Wei W, Liu H, Ma J, Hu M, Huang H. Acute response of neurons: an early event of neuronal cell death after facial nerve injury. World Neurosurg. 2018;109:e252–7. https://doi.org/10.1016/j.wneu.2017.09.157.
78. Xue R, Xie M, Wu Z, Wang S, Zhang Y, Han Z, et al. Mesenchymal stem cell-derived exosomes promote recovery of the facial nerve injury through regulating macrophage M1 and M2 polarization by targeting the P38 MAPK/NF-Kb pathway. Aging Dis. 2024;15(2):851–68. https://doi.org/10.14336/ad.2023.0719-1.
79. Chowen JA, Garcia-Segura LM. Role of glial cells in the generation of sex differences in neurodegenerative diseases and brain aging. Mech Ageing Dev. 2021. https://doi.org/10.1016/j.mad.2021.111473.
80. Fex Svenningsen A, Kanje M. Estrogen and progesterone stimulate Schwann cell proliferation in a sex- and age-dependent manner. J Neurosci Res. 1999;57(1):124–30.

Publisher's Note Springer Nature remains neutral with regard to jurisdictional claims in published maps and institutional affiliations.

Springer Nature or its licensor (e.g. a society or other partner) holds exclusive rights to this article under a publishing agreement with the author(s) or other rightsholder(s); author self-archiving of the accepted manuscript version of this article is solely governed by the terms of such publishing agreement and applicable law.